École polytechnique fédérale de Lausanne (EPFL)

Faculté des sciences de base
Section de physique

Centre de Recherches en Physique des Plasmas (CRPP)

Association EURATOM
Confédération Suisse

Neutral particle analysis (NPA)

Error Estimation and Parameter Dependence of the Calculation of the Fast Ion Distribution Function, Temperature and Density Using Data From the KF1 High Energy NPA on JET

Christian SCHLATTER

UKAEA Fusion Association
EFDA-JET CSU, Building K1
Culham Science Centre
Abingdon, OXFORDSHIRE, OX14 3EA, UK

2004, 5^{th} of January

Made with LaTeX 2_ε

Abstract

The high energy neutral particle analyzer at JET provides information on the absolute value of the fast ions energy distribution function near the plasma centre, from which the fast ion temperature and density can be obtained. The derivation of these quantities from the flux of detected neutral particles is based both on measured global plasma parameters such as the density, temperature and effective charge and on the estimated particle confinement time, as well as on the knowledge of the cross-section for the relevant collision mechanisms such as charge-exchange and recombination with impurities. The effect of uncertainties in the plasma parameters in the evaluation of the fast ion energy distribution function, temperature and density is reported here. The results of this study indicate that the most important parameters affecting the absolute value of the energy distribution function are the impurity confinement time and, to a minor extent, the impurity concentration. On the other hand, the fast ion temperature is not particularly affected unless clearly non-physical values of the input parameters are used. Benchmark with independent magnetic measurement of the fast ion energy are then used to refine the choice of the input data used in the neutralization calculation. In conclusion, this study confirm the robustness of the JET high energy NPA as a tool for the measurement of the fast ion temperature and density in the plasma core as well as individuating in the impurity confinement time and concentration the physical quantities that require a better estimate.

This abstract has been submitted to the 15^{th} topical conference on high-temperature plasma diagnostics in San Diego, California, USA (19^{th} to 22^{nd} of April 2004).

Contents

Chapter 1

Parameter dependence

1.1 Introduction

In the aim to understand the sensitivity of JET's code calculating the neutralization probability on its various input parameters an extensive analysis has been carried out.

KF1 is JET's high energy neutral particle analyzer[(1)] (NPA) measuring neutral flux of hydrogen and helium isotopes[(2)] of energies ranging from approximately 200 keV to 4 MeV. The diagnostic has a vertical line of sight (from top to down in octant 4 at a radial position of R = 3.07 m, see figure 1.1) which intersects the horizontal NBI beam in octant 4. From its measurements the fast ion distribution function $f_i^{fast}(E)$, the fast ion perpendicular[(3)] temperature $T_{i,\perp}^{fast}$ and the fast ion density n_i^{fast} can be derived.

For the present work one single plasma discharge has been selected, namely shot #61260 of the 2003 trace tritium campaign[(4)] C11.

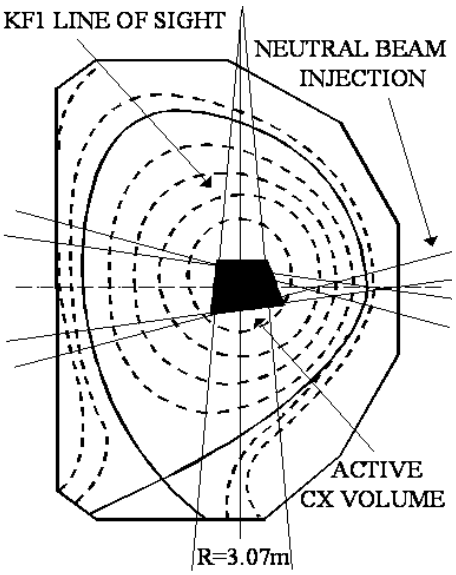

Figure 1.1: NPA line of sight and its intersection with the neutral beam (NBI).

(1) model GEMMA-2M, developed by the Ioffe institute, St. Petersburg. Operational since the early nineties.
(2) H, D, T, ^{3}He, ^{4}He, but only one at a time.
(3) The line of sight is perpendicular to the magnetic field, only particles with a $\frac{v_\perp}{v_\parallel} \approx 200$ are detected.
(4) H-9.2.1: Investigation of pT fusion with hydrogen minority heating, carried out on the 9^{th} of October.

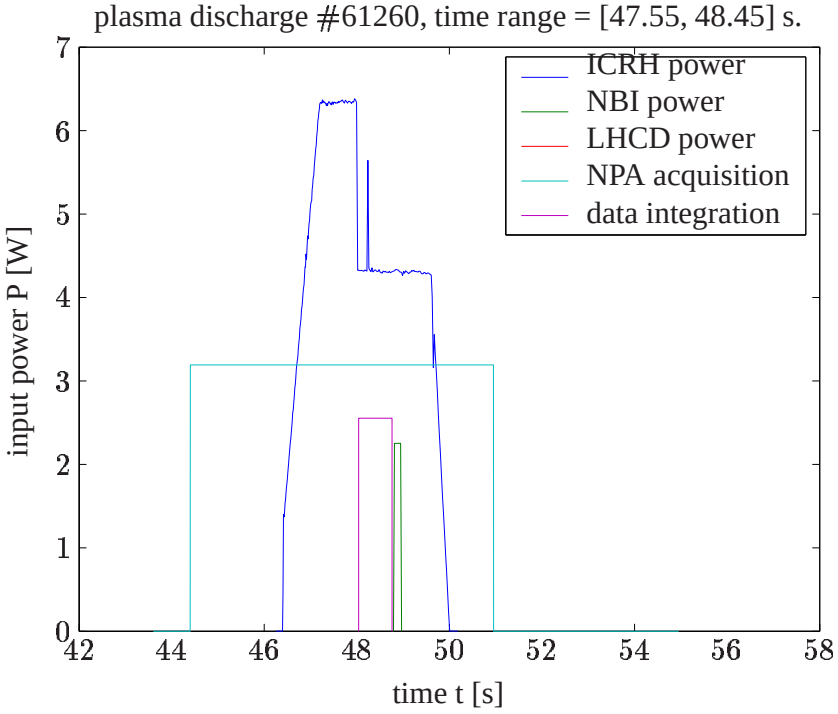

Figure 1.2: ICRF and NBI injected power for JET discharge #61260. The NPA data acquisiton is indicated with the cyan window, for the data analysis in this work the time interval marked in violet has been considered only. There was no lower hybrid current drive in this discharge.

The ICRF heating was tuned to the H-minority at its 1^{st} harmonic. The toroidal magnetic field was $B_T = 3.4$ T, plasma current $I_p = 1.8$ MA, electron temperature $T_e = 7$ keV, electron density $n_e = 3{\cdot}10^{-19}$ m^{-3}, diamagnetic energy $W_{DIA} = 2.5$ MJ.

1.2 Measurement of the neutral flux

Figure 1.2 shows input power versus time for this shot. For statistical reasons the neutral flux used in the following was integrated over the time-window indicated in violet ($t \in [47.55, 48.45]$ s). For this period the ICRF heating power (blue curve) was fairly constant and there was no NBI activity (green). The cyan curve shows the time-window where the data acquisition of the NPA was working for this discharge.

The pulse height analysis for the eight NPA channels of the registered counts is shown in figure 1.3. As it can be seen, the counts due to the neutrons[(5)] are well rejected[(6)] by the good selection of the lower threshold (ADC channel one) of the pulse-height analysis. Extending the lower pulse intensity limit towards smaller values would show large counts in the lower ADC channels, what has to be avoided. The upper limit is ideally chosen to have almost zero counts in the uppermost channel[(7)]; in channel 4 there are a lot of pulses accumulated in ADC channel 16 due to a too small upper pulse height limit. This is not dramatic, since all pulses

(5) The energy deposited in the scintillators by neutrons is much smaller than that by charged particles, leading to a smaller scintillator light yield

(6) look at channel 5 or 8.

(7) see channel 8.

exceeding the upper limit are accounted for in ADC channel 16. The present calibration of the NPA system exhibits problems for channel one (reduced overall sensitivity) and channel 7 (fairly non-gaussian pulse-height spectrum). These problems will be addressed during the major shutdown of JET in 2004/2005.

The combination of the integrals over the ADC channels of the eight plots of figure 1.3 are shown in figure 1.4 (left plot), for clarity the errorbars in counts are shown explicitly on the right plot, they are determined by the assumption that the counts are distributed following a Poisson statistics.

1.3 Inferred $f_i^{fast}(E)$, $\overline{T_\perp^{fast}}$ and n_i^{fast}

1.3.1 Fast ion distribution function

How can now the fast ion distribution function $f_i^{fast}(E)$ be addressed from the measured neutral counts $N(E)$? Lets quickly review how the neutral flux is issued: The fast ions in the plasma, described by their distribution function $f_i^{fast}(E)$ can only be diagnosed when they became neutrals, as charged particles can not escape the plasma due to their confinement within the magnetic field. The neutralization of the ions is described by the neutralization probability $P_\nu(E)$. On their way across the magnetic surfaces, the neutrals can be reionized again, what is quantized by the reionization probability $\gamma(E)$ (aka plasma transparency). The quantity

$$\Gamma(E) = \frac{f_i^{fast}(E)}{\gamma(E) \cdot P_\nu(E)}$$

can therefore be interpreted as the neutral flux escaping the plasma column. The part of the flux of neutrals with energy E entering the solid angle Ω of the NPA detectors with étendue (ΩS) is registered with a detection efficiency $\mu_j(E)$, where the j^{th} channel energy width ΔE_j has to be taken into account. The encountered neutral counts $N_j(E)$ in the NPA channel measuring at energy E_j is therefore related to $f_i^{fast}(E)$ by the following formula:

$$N_j(E) = (\Omega S) \cdot \Delta E_j \cdot \mu_j(E) \cdot \gamma(E) \cdot P_\nu(E) \cdot f_i^{fast}(E) \tag{1.1}$$

Whereas the detector parameters are well known, a model is needed for the calculation of the neutralization and reionization probabilities. On JET the **I**mpurity **I**nduced **N**eutralization model (**IIN**) was developed for this purpose ([3] by Korotkov et al.). IIN includes radiative recombination with electrons, charge exchange reactions with impurities, thermal deuterium and NBI atoms and equates a system of steady-state ion density balance equations for bare, [H]-, and [He]-like impurities. The required input parameters are impurity (He, Be, C) density ratios and their respective confinement times, the ion temperature T_i, the electron density n_e, the thermal deuterium density $n_D^{thermal}$ and the effective charge Z_{eff}.

Figure 1.5 shows the neutral particle flux established from the counts shown in figure 1.4, the neutralization and reionization probabilities calculated using the IIN model and finally the inferred fast ion distribution function calculated using equation 1.1.

As pointed out in [1], the main source of uncertainties for the determination of the fast ion distribution function is the [H]-like electron donor density in the plasma core, which results in an uncertainty of 45 % in the neutralization probability. According to equation 1.1, the errorbar on $f_i^{fast}(E)$ is about

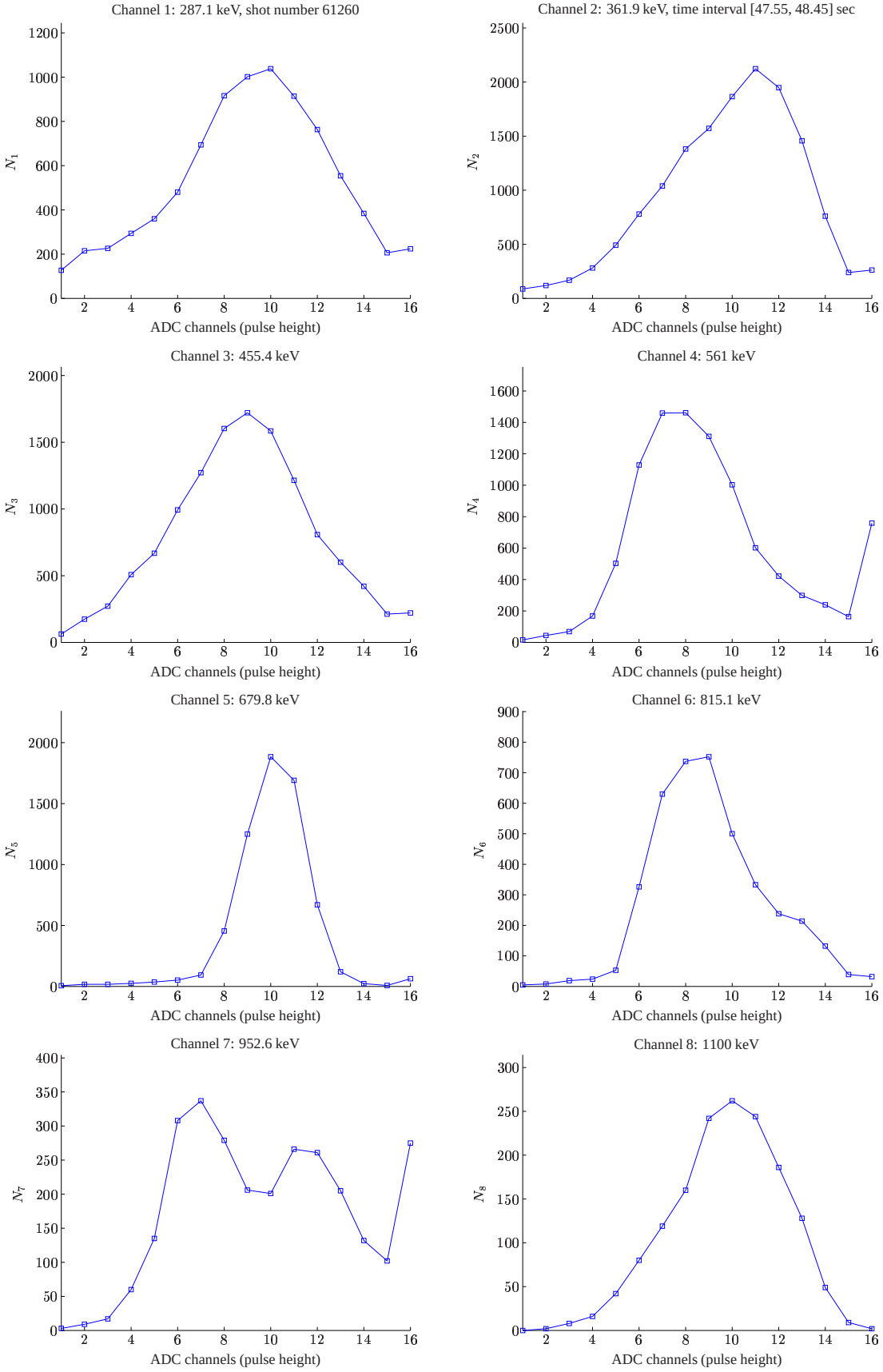

Figure 1.3: Pulse height analysis for the eight NPA channels. In the present configuration there is no contribution to the counts due to the neutrons.

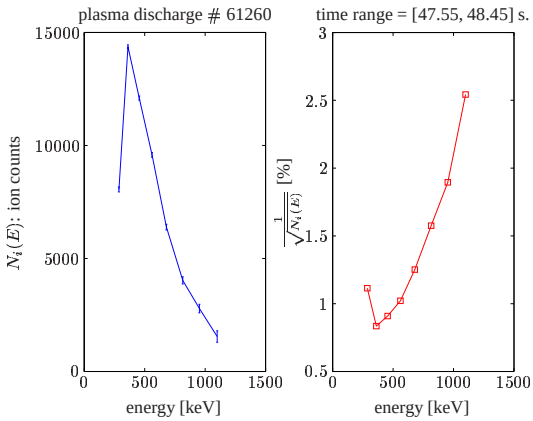

Figure 1.4: Integrated neutral counts against NPA channel energy (left plot). The plot on the right side shows the associated errorbars adopting Poisson statistics.

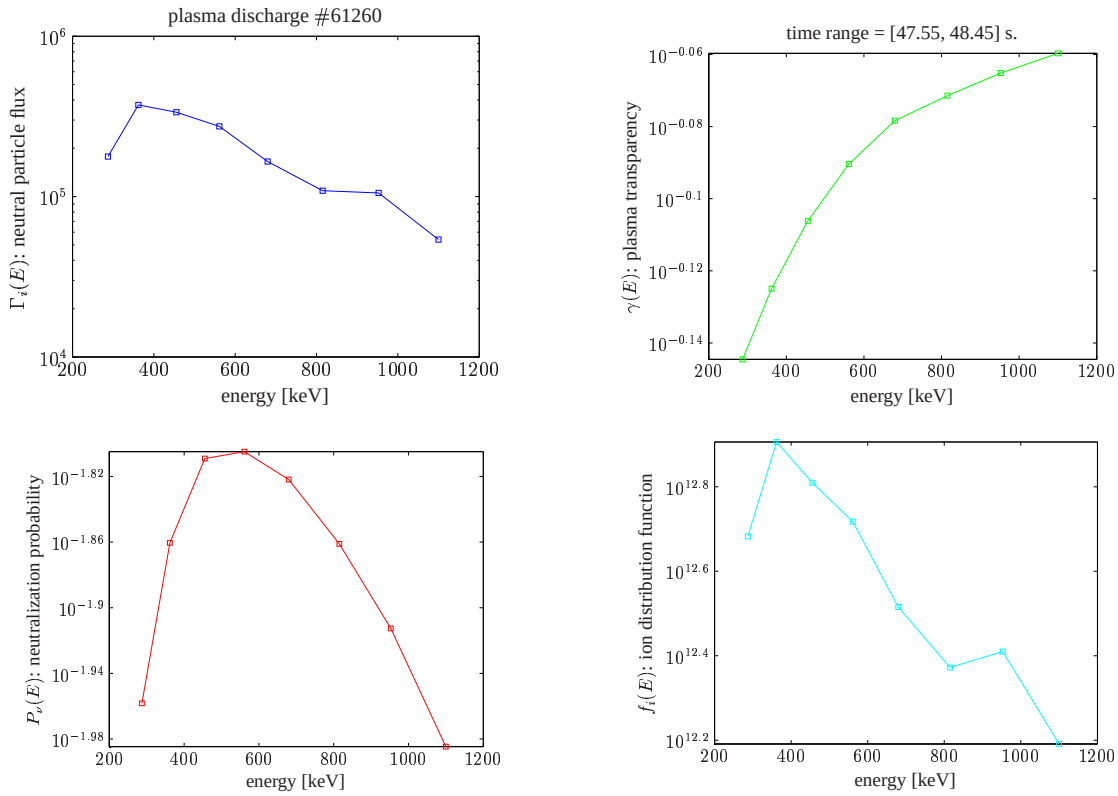

Figure 1.5: With the neutral counts integrated over the time interval $t \in [47.55, 48.45]$ s for discharge #61260 shown in figure 1.4 from the upper left to the lower right are plotted: The fast neutral particle flux $\Gamma_i(E)$, the plasma transparency $\gamma(E)$, the fast ion neutralization probability $P_\nu(E)$ and the inferred fast ion distribution function $f_i^{fast}(E)$.

$$\frac{\Delta\overline{f_i^{fast}}}{\overline{f_i^{fast}}} \approx \sqrt{\left(\frac{\Delta P_\nu}{P_\nu}\right)^2 + \left(\frac{\Delta\gamma}{\gamma}\right)^2 + \left(\frac{\Delta\mu}{\mu}\right)^2 + \left(\frac{\Delta N_i^{fast}}{N_i^{fast}}\right)^2} = \tag{1.2}$$

$$\sqrt{0.45^2 + 0.15^2 + 0.1^2 + 0.05^2} \approx 50\%$$

1.3.2 Fast ion perpendicular temperature

The fast ion perpendicular temperature $\overline{T_{i\perp}^{fast}}$ is inferred from the fast ion distribution function using Stix's expression [5] for ICRF heated ions, namely

$$\overline{f_i^{fast}}(E) \sim \frac{\sqrt{E}}{\overline{T_{i\perp}^{fast}}} \exp\left(-\frac{E}{\overline{T_{i\perp}^{fast}}}\right) \tag{1.3}$$

and therefore the perpendicular fast ion temperature can be inferred from the slope of the logarithm of the fast ion distribution function, i.e.

$$-\frac{1}{\overline{T_{i\perp}^{fast}}} = \frac{\partial}{\partial E} \ln\left(\frac{\overline{f_i^{fast}}(E)}{\sqrt{E}}\right) \tag{1.4}$$

where the bars over the quantities $\overline{f_i^{fast}}(E)$ and $\overline{T_{i\perp}^{fast}}(E)$ stand for line-of-sight integrated values.

The central fast ion perpendicular temperature $T_{i\perp}^{fast}(r=0)$ is then given by the formula stated in [4], i.e.

$$T_{i\perp}^{fast}(r=0) \simeq \overline{T_{i\perp}^{fast}}(E^*)\left(1 + \frac{\overline{T_{i\perp}^{fast}}(E^*)}{2E^*}\right) \tag{1.5}$$

where E^* is the median energy of the range of measurements. Figure 1.6 shows the least square fit to the logarithm of the fast ion distribution function, for which the data points for NPA channel 1 and 7 have been excluded for the reason of the calibration issues mentioned in section 1.2. The slope of the fit gives $\overline{T_{i\perp}^{fast}} = 421$ keV and formula 1.5 yields $T_{i\perp}^{fast}(r=0) = 555$ keV (#61260, $t \in [47.55, 48.45]$ s).

The errorbars on the fast perpendicular ion temperature are fairly low, since the main source of uncertainty on the temperature are the calculated C^5-ions charge exchange cross-section (20 %), resulting in [1]

$$\frac{\Delta T_{i\perp}^{fast}}{T_{i\perp}^{fast}} \approx 2 \cdot 10^{-3} \frac{\Delta\sigma_{CX}}{\sigma_{CX}} T_{i\perp}^{fast} \approx 10\,\% \tag{1.6}$$

1.3.3 Fast ion density

From the line integrated fast ion distribution function it is straightforward to deduce the fast ion density by integrating $f_i(E)$ over the energy range of the measurement, i.e. by

$$\overline{n_i^{fast}} = \frac{1}{E_{max} - E_{min}} \int_{E_{min}}^{E_{max}} \overline{f_i(E)}\, dE \tag{1.7}$$

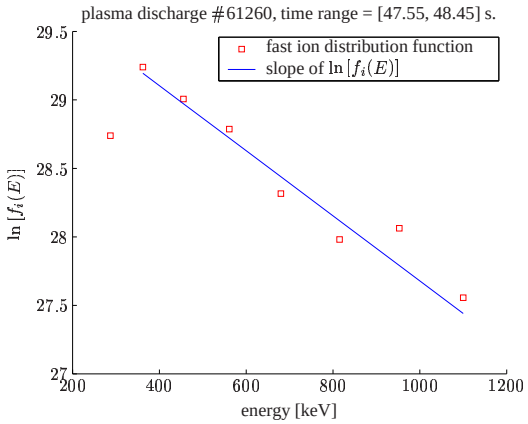

Figure 1.6: Inferred temperature for the fast ion distribution function shown in figure 1.5. $\overline{T_{i\perp}^{fast}} = 421$ keV, $T_{i\perp}^{fast}(r=0) = 555$ keV

This procedure results in a fast ion density of $\overline{n_i^{fast}} = 2.3 \cdot 10^{18} m^{-3}$ for the distribution function shown in figure 1.5.

The way the fast ion density is calculated requires to set the errorbars identically with those for the fast ion distribution function, i.e. 50 % [1], [6].

1.4 Neutralization input parameter analysis

So far the plots shown were established using the input data from the JET database or default initial guess or calculation of quantities which are not measured. What happens when a input parameter is modified, especially within its errorbar?

1.4.1 Fast ion distribution function

Figure 1.7 shows a compilation of such a procedure for the NPA data of discharge #61260 in the time window $[47.55, 48.45]$ s and its effect on the resulting fast ion distribution function. The modified parameters and its associated errorbars were the following: The relative impurity concentrations (Beryllium over carbon Be/C and Helium over carbon ratio $He/C \pm 100\%$), the thermal deuterium density $n_D \pm 100\%$, the electron density $n_e \pm 20\%$, the empirical impurity confinement times τ for Beryllium, Helium and Carbon $\pm 100\%$, the ion temperature $T_i \pm 10\%$, the effective charge $Z_{eff} \pm 30\%$ and the statistical Poisson error (see figure 1.4) of the fast neutral counts N_i.

It is found that the modification of most of the input parameters within their errorbars doesn't change the absolute value of the fast ion distribution function remarkably. Dramatic changes result when decreasing the impurity confinement times towards zero, but this makes physically not much sense (see later). Especially the confinement of carbon and to a minor extent Beryllium change the neutralization probability and therefore f_i^{fast} by 2 and 1 order of magnitude respectively. The modified shape of f_i^{fast} by changing τ_{Be} or τ_{He} are due to the stronger energy dependence of the cross-sections for charge exchange [3]. Z_{eff} affects neutralization and reionization (see the impact on $\gamma(E)$), which is also seen in f_i^{fast}.

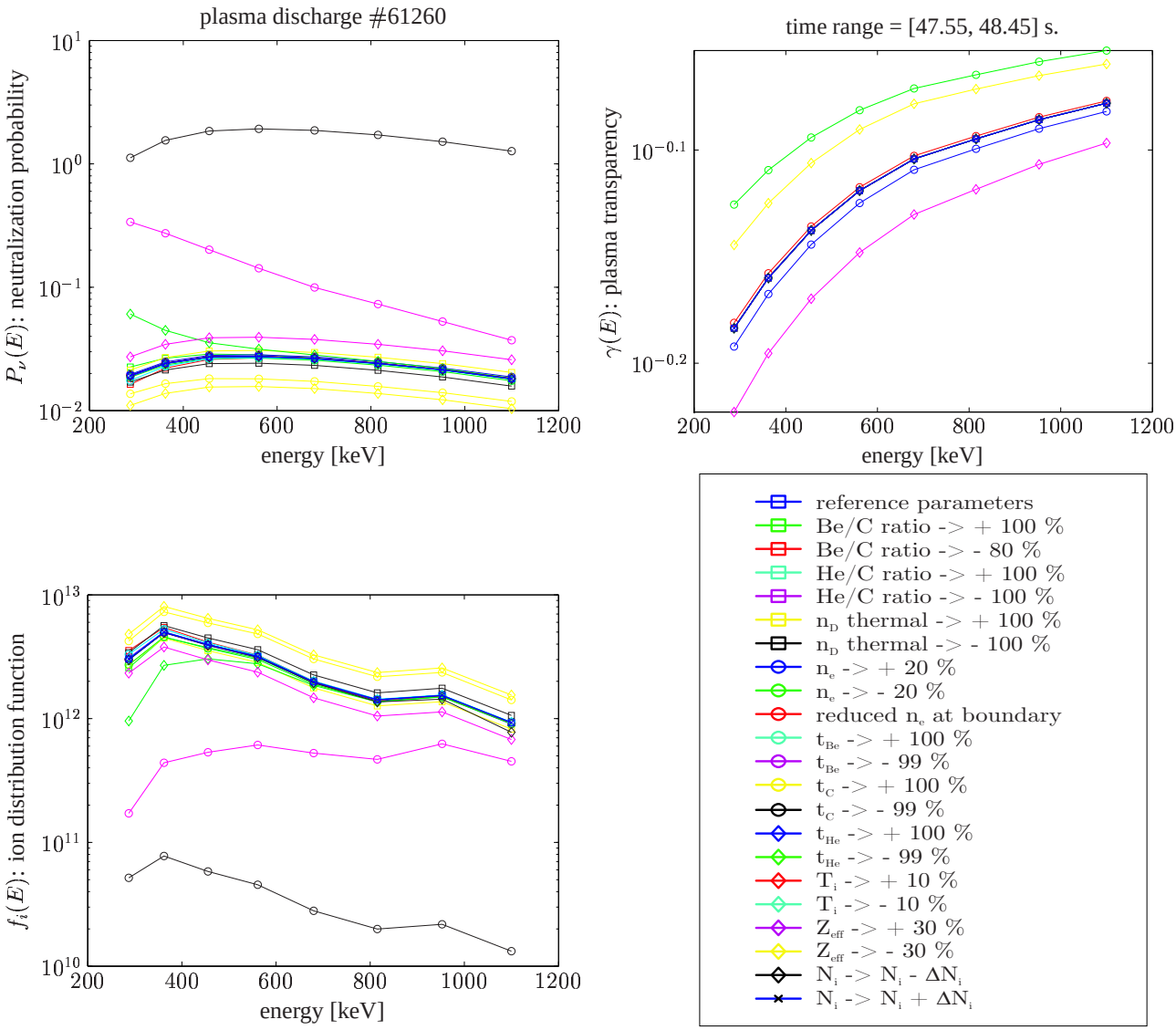

Figure 1.7: Neutralization code input parameter impact on the calculation of neutralization probability and the plasma transparency. The lower left plot shows how the inferred fast ion distribution function is modified.

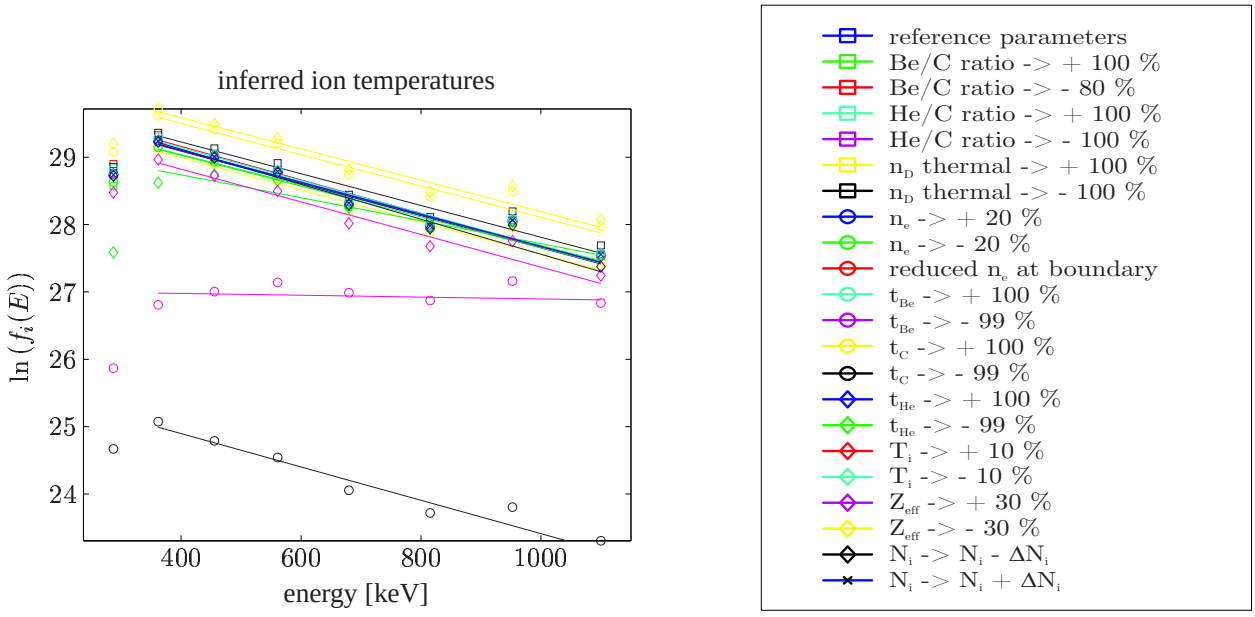

Figure 1.8: Neutralization code input parameter impact on the fast ion temperature fit.

1.4.2 Fast ion temperature

As exposed in the previous section, the fast ion temperature only depends on the slope of f_i^{fast}. Since most of the input parameter only affect the absolute value of $f_{i,fast}$, the impact on the inferred fast ion temperature is rather weak. Figure 1.8 shows and table 1.1 lists how the changed input parameters are reflected in the fast ion temperature. Apart from the two non-physical impurity confinement times τ_C and $\tau_{Be} \rightarrow 0$, the inferred temperature is indeed very insensitive to the modified parameters, with changes inferior to $\pm$ 10 %.

1.4.3 Fast ion density

Table 1.2 shows the values of the fast ion density obtained when applying the formula 1.7 to the data shown in figure 1.7. The thermal deuterium density, the effective charge and above all the ion confinement times affect the fast ion density.

1.4.4 Impurity confinement times

In the previous sections it was seen that the impurity confinement times are the dominant parameter in the calculation of the ion distribution function. To better understand the impact of the τ_{Be} and τ_C, a further scan of these parameters was carried out. Figure 1.9 and table 1.3 show how the fast ion distribution function, temperature and density are altered when modifying τ_{Be} in the range of $[0, 2]$ s.

A simple estimation of τ can be derived from transport, i.e.

$$\Gamma_Z = -Dn'_Z + \frac{r}{a} v n_Z \tag{1.8}$$

To the impurity of atomic charge Z it is attributed a confinement time

$$\tau_Z = \frac{n_Z}{div\Gamma_Z} \tag{1.9}$$

modified input parameter			$\overline{T_\perp}$ [keV]	$T_\perp(r=0)$ [keV]	$\frac{\Delta T_\perp(r=0)}{T_\perp^{ref}(r=0)}$ [%]
reference parameters			421.0	554.8	0.0
Be/C ratio	$\rightarrow$	+ 100 %	444.5	593.7	5.6
Be/C ratio	$\rightarrow$	- 80 %	401.9	523.9	-4.5
He/C ratio	$\rightarrow$	+ 100 %	422.7	557.7	0.4
He/C ratio	$\rightarrow$	- 100 %	419.3	552.0	-0.4
n_D thermal	$\rightarrow$	+ 100 %	418.7	551.1	-0.6
n_D thermal	$\rightarrow$	- 100 %	423.7	559.3	0.7
n_e	$\rightarrow$	+ 20 %	417.7	549.4	-0.8
n_e	$\rightarrow$	- 20 %	436.8	580.8	3.8
reduced n_e at boundary			421.6	555.8	0.1
τ_{Be}	$\rightarrow$	+ 100 %	411.0	538.5	-2.4
τ_{Be}	$\rightarrow$	- 99 %	7286.9	47379.2	1630.9
τ_C	$\rightarrow$	+ 100 %	430.2	569.9	2.2
τ_C	$\rightarrow$	- 99 %	404.2	527.6	-4.0
τ_{He}	$\rightarrow$	+ 100 %	420.2	553.5	-0.2
τ_{He}	$\rightarrow$	- 99 %	587.3	847.7	39.5
T_i	$\rightarrow$	+ 10 %	420.8	554.6	0.0
T_i	$\rightarrow$	- 10 %	421.2	555.1	0.1
Z_{eff}	$\rightarrow$	+ 30 %	412.5	540.9	-2.0
Z_{eff}	$\rightarrow$	- 30 %	429.5	568.8	2.0
N_i	$\rightarrow$	$N_i - \frac{1}{\sqrt{(N_i)}}$	384.6	496.2	-8.7
N_i	$\rightarrow$	$N_i + \frac{1}{\sqrt{(N_i)}}$	457.8	616.0	8.7

Table 1.1: The impact of input parameter modification on the fast ion temperature

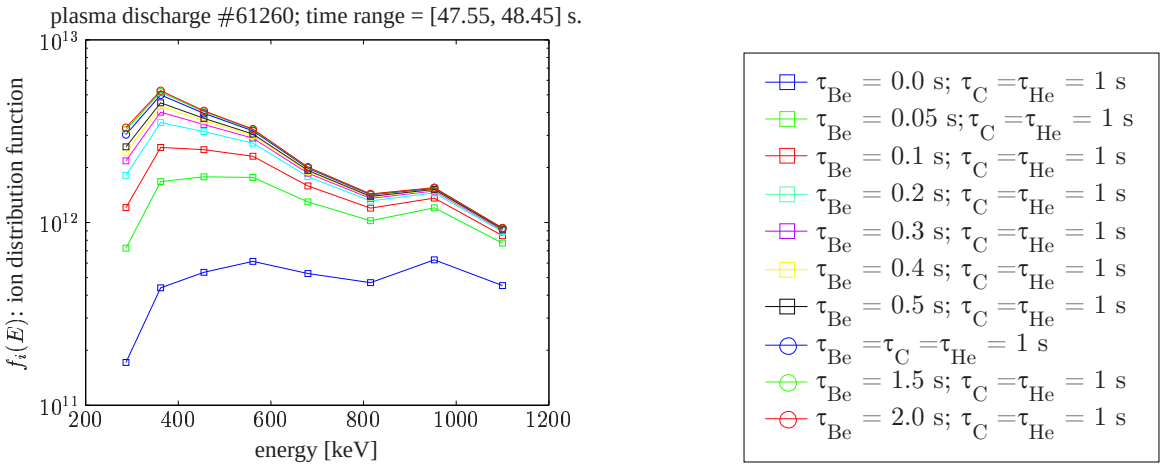

Figure 1.9: Impact of τ_{Be} on the fast ion distribution function. The inferred temperatures are shown in table 1.3.

modified input parameter			n_i^{fast} [m^{-3}]	$\frac{\Delta n_i^{fast}}{n_i^{fast}}$ [%]
reference parameters			$2.3{\cdot}10^{18}$	0.0
Be/C ratio	$\rightarrow$	+ 100 %	$2.2{\cdot}10^{18}$	-3.2
Be/C ratio	$\rightarrow$	- 80 %	$2.4{\cdot}10^{18}$	2.9
He/C ratio	$\rightarrow$	+ 100 %	$2.3{\cdot}10^{18}$	-0.1
He/C ratio	$\rightarrow$	- 100 %	$2.3{\cdot}10^{18}$	0.1
n_D thermal	$\rightarrow$	+ 100 %	$2.1{\cdot}10^{18}$	-10.7
n_D thermal	$\rightarrow$	- 100 %	$2.6{\cdot}10^{18}$	13.6
n_e	$\rightarrow$	+ 20 %	$2.3{\cdot}10^{18}$	-1.7
n_e	$\rightarrow$	- 20 %	$2.2{\cdot}10^{18}$	-5.2
reduced n_e at boundary			$2.3{\cdot}10^{18}$	-0.4
τ_{Be}	$\rightarrow$	+ 100 %	$2.3{\cdot}10^{18}$	2.3
τ_{Be}	$\rightarrow$	- 99 %	$5.3{\cdot}10^{17}$	-76.8
τ_C	$\rightarrow$	+ 100 %	$3.5{\cdot}10^{18}$	51.2
τ_C	$\rightarrow$	- 99 %	$3.3{\cdot}10^{16}$	-98.6
τ_{He}	$\rightarrow$	+ 100 %	$2.3{\cdot}10^{18}$	0.1
τ_{He}	$\rightarrow$	- 99 %	$1.9{\cdot}10^{18}$	-15.7
T_i	$\rightarrow$	+ 10 %	$2.3{\cdot}10^{18}$	-0.5
T_i	$\rightarrow$	- 10 %	$2.3{\cdot}10^{18}$	0.6
Z_{eff}	$\rightarrow$	+ 30 %	$1.7{\cdot}10^{18}$	-25.4
Z_{eff}	$\rightarrow$	- 30 %	$3.8{\cdot}10^{18}$	64.4
N_i	$\rightarrow$	$N_i - \frac{1}{\sqrt{(N_i)}}$	$2.2{\cdot}10^{18}$	-2.9
N_i	$\rightarrow$	$N_i + \frac{1}{\sqrt{(N_i)}}$	$2.3{\cdot}10^{18}$	0.0

Table 1.2: The impact of input parameter modification on the fast ion density.

τ_{Be} [s]	$T_\perp(r=0)$ [keV]	$\frac{\Delta T_\perp(r=0)}{T_\perp^{ref}(r=0)}$ [%]	n_i^{fast} [m^{-3}]	$\frac{\Delta n_i^{fast}}{n_i^{fast}}$ [%]
0.00	47379.2	1630.9	$0.5{\cdot}13^{18}$	-76.8
0.05	1328.4	94.9	$1.3{\cdot}13^{18}$	-42.2
0.10	875.3	43.0	$1.6{\cdot}18^{18}$	-26.9
0.20	690.0	18.9	$1.9{\cdot}16^{18}$	-14.6
0.30	632.5	11.0	$2.0{\cdot}18^{18}$	-9.2
0.40	604.4	7.1	$2.1{\cdot}15^{18}$	-6.2
0.50	587.9	4.8	$2.2{\cdot}10^{18}$	-4.3
1.00	**554.8**	**0.0**	$2.3{\cdot}10^{18}$	**0.0**
1.50	543.8	-1.6	$2.3{\cdot}13^{18}$	1.6
2.00	538.5	-2.4	$2.3{\cdot}15^{18}$	2.3

Table 1.3: Impact of τ_{Be} on the fast ion temperature and density.

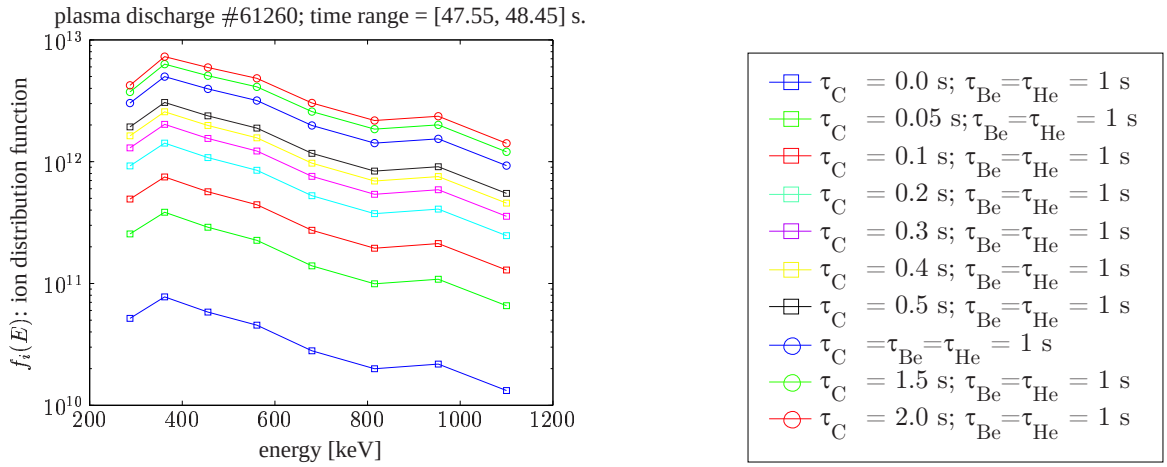

Figure 1.10: Impact of τ_C on the fast ion distribution function. The inferred temperatures are shown in table 1.4.

τ_C [s]	$T_\perp(r=0)$ [keV]	$\frac{\Delta T_\perp(r=0)}{T_\perp^{ref}(r=0)}$ [%]	n_i^{fast} [m^{-3}]	$\frac{\Delta n_i^{fast}}{n_i^{fast}}$ [%]
0.00	527.6	-4.0	$3.3{\cdot}10^{16}$	-98.6
0.05	528.7	-3.8	$1.7{\cdot}10^{17}$	-92.8
0.10	530.6	-3.5	$3.2{\cdot}10^{17}$	-85.9
0.20	534.1	-3.0	$6.2{\cdot}10^{17}$	-73.0
0.30	537.3	-2.6	$8.9{\cdot}10^{17}$	-61.2
0.40	540.4	-2.1	$1.1{\cdot}10^{18}$	-50.4
0.50	543.2	-1.7	$1.4{\cdot}10^{18}$	-40.4
1.00	554.8	0.0	$2.3{\cdot}10^{18}$	0.0
1.50	563.6	1.3	$3.0{\cdot}10^{18}$	29.2
2.00	569.9	2.2	$3.5{\cdot}10^{18}$	51.2

Table 1.4: Impact of τ_C on the fast ion temperature and density.

It is found that $\tau_Z \approx 1$ s for JET conditions [1].

Beryllium

From figure 1.9 it is found that around $\tau_{Be} \approx 1$ s the fast ion temperature and density do change only marginally and therefore the sensitivity of the calculations on τ_{Be} may be neglected.

Carbon

Another picture is revealed when modifying τ_C. As shown in figure 1.10 there is no very clear saturation of the absolute value of the fast ion distribution function in τ_C.
Indeed the dependence on τ_C is weaker around 1 s (figure 1.11), but a modification of τ_C by $\sim$ 50 % results still in a change in density of about 30 %. However the fast ion temperature is not affected (see table 1.4).

There are other methods to infer the fast ion density which gives the possibility for comparisons with the value obtained here. Spectroscopy measures the ratio of the emission line intensities

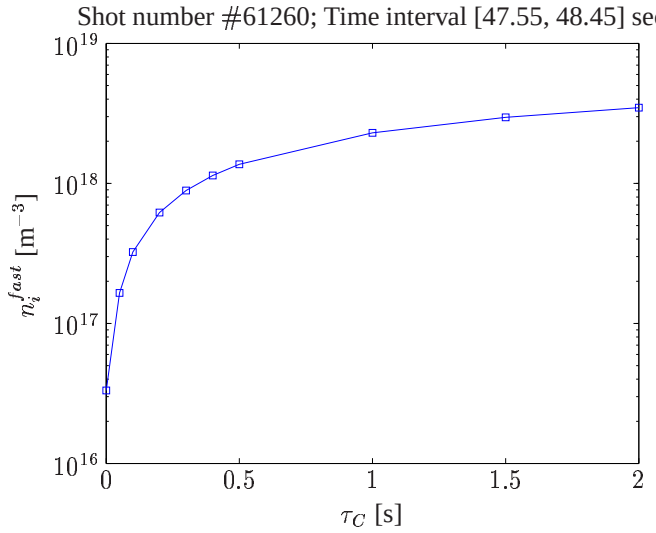

Figure 1.11: Dependence of the inferred fast ion density on the carbon confinement time τ_C.

of the hydrogenic species, i.e

$$\alpha = \frac{H_\alpha}{H_\alpha + D_\alpha + T_\alpha} \tag{1.10}$$

what, supposing $n_D \approx n_e$, is approximately

$$\alpha \approx \frac{n_H}{n_H + n_D + n_T} \tag{1.11}$$

therefore, for ICRF tuned to the hydrogen minority,

$$n_i^{fast} \approx \frac{\alpha}{1-\alpha} \tag{1.12}$$

which gives $n_i^{fast} \pm 1.5 \cdot 10^{18}$ m^{-3} $\pm$ 30 % for the shot and time interval considered.

Another approach is given by the measurement of the fast particle energy, which is determined by [2][(8)]

$$W_{fast} = \frac{4}{3}\left(W_{DIA} - W_{MHD}\right) \tag{1.13}$$

where W_{DIA} is the plasma energy measured by the diamagnetic loop and W_{MHD} is calculated by JET's equilibrium reconstruction code EFIT using magnetic measurements and MHD calculations. Knowing W_{fast}, the fast ion density n_i^{fast} is then obtained using

$$W_{fast} = 4\pi^2 R_0 \int_0^a r\,\kappa(r)\, n_i^{fast}(r) \left[T_{i\perp} + \frac{1}{2}T_{i\parallel}\right] dr \tag{1.14}$$

Using gaussian density and temperature profiles with a width of $\Delta = 0.3$ m, the limiter a = 1.2 m and the usual assumption that $T_{i\parallel} = 0.1 \cdot T_{i\perp}$, a resulting $n_i^{fast} = 9.0 \cdot 10^{17}$ m^{-3} $\pm$ 30 % is found for the shot and time interval considered.

With the cited precisions of the calculations of n_i^{fast} using spectroscopic measurements, agreement with the density inferred from the fast ion distribution function is found. This confirms the estimate of τ_C. By contrast, the fast ion energy approach gives a value that is almost 50 % lower (see figure 1.12).

(8) equation 10 in [2] is wrong: W_{fast} is found combining equations 11 and 12 therein using $W_{fast} = W_\perp - 2W_\parallel$

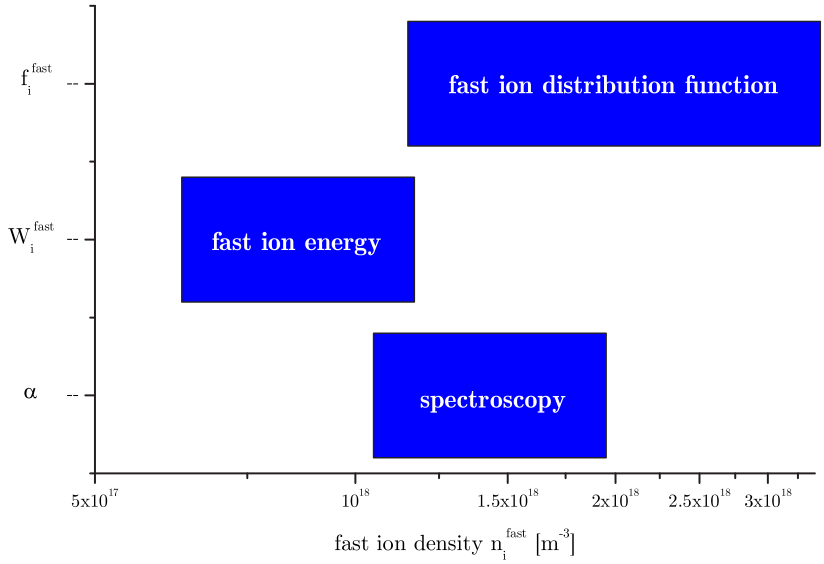

Figure 1.12: Comparison of the fast ion density determined using spectroscopic measurements (uncertainty ± 30 %), the fast ion energy (± 30 %) or the fast ion distribution function (± 50 %). The length of the bars correspond to the errorbars.

1.5 Conclusion

The present work outlined the reliable and robust measurement of the fast ion perpendicular temperature $T_{i\perp}$ using experimental data from the high energy NPA KF1.

The crude **IIN**-model permits to calculate the fast ion density n_i^{fast} with 50 % of uncertainty, with a refined analysis of the neutralization calculation input parameter the errorbars may be reduced well below. The inference of n_i^{fast} from NPA data is in agreement with edge spectroscopy measurements.

The behavior of the NPA channel 1 and 7 in recent experimental campaigns demonstrates the necessity of a refurbishment and recalibration of the diagnostic to ensure the reliability of the measurements.

Bibliography

[1] A.A.Korotkov, A.Gondhalekar, and A.J.Stuart, *Impurity induced neutralization of mega-electronvolt energy protons in jet plasmas*, Nuclear Fusion **37** (1997), no. 1, 35–51.

[2] L.-G. Eriksson, T. Hellsten, and U. Willén, *Comparison of time dependent simulations with experiments in ion cyclotron heated plasmas*, Nucl. Fusion **33** (1993), no. 7, 1037–1048.

[3] A. A. Korotkov and A. Gondhalekar, *Impurity induced neutralization of mev energy protons in jet plasmas*, preprint of a paper submitted for publication in Nuclear Fusion JET-P(95)47, JET Joint Undertaking, Abingdon, Oxfordshire, OX14 3EA, United Kingdom, September 1995.

[4] K. G. McClements, R. O. Dendy, and A. Gondhalekar, *Interpretation of measurements of icrf heated minority proton distributions in jet*, Nuclear Fusion **37** (1997), no. 4, 473–480.

[5] Thomas Howard Stix, *Fast-wave heating of a two-component plasma*, Nuclear Fusion **15** (1975), no. 5, 737–754.

[6] Duccio Testa and A. Gondhalekar, *Fast ion density measurements using high energy neutral particle analysis in jet*, Nuclear Fusion **40** (2000), no. 5, 975–988.